3172–3182 Nucleic Acids Research, 2012, Vol. 40, No. 7 Published online 1 December 2011
doi:10.1093/nar/gkr1143

Solution structure of the dimerization domain of the eukaryotic stalk P1/P2 complex reveals the structural organization of eukaryotic stalk complex

Ka-Ming Lee[1], Conny Wing-Heng Yu[1], Teddy Yu-Hin Chiu[1], Kong-Hung Sze[2], Pang-Chui Shaw[1] and Kam-Bo Wong[1,*]

[1]School of Life Sciences, Centre for Protein Science and Crystallography, The Chinese University of Hong Kong and [2]Department of Chemistry, University of Hong Kong, Hong Kong, China

Received April 15, 2011; Accepted November 8, 2011

ABSTRACT

The lateral ribosomal stalk is responsible for the kingdom-specific binding of translation factors and activation of GTP hydrolysis during protein synthesis. The eukaryotic stalk is composed of three acidic ribosomal proteins P0, P1 and P2. P0 binds two copies of P1/P2 hetero-dimers to form a pentameric P-complex. The structure of the eukaryotic stalk is currently not known. To provide a better understanding on the structural organization of eukaryotic stalk, we have determined the solution structure of the N-terminal dimerization domain (NTD) of P1/P2 hetero-dimer. Helix-1, -2 and -4 from each of the NTD-P1 and NTD-P2 form the dimeric interface that buries 2200 A^2 of solvent accessible surface area. In contrast to the symmetric P2 homo-dimer, P1/P2 hetero-dimer is asymmetric. Three conserved hydrophobic residues on the surface of NTD-P1 are replaced by charged residues in NTD-P2. Moreover, NTD-P1 has an extra turn in helix-1, which forms extensive intermolecular interactions with helix-1 and -4 of NTD-P2. Truncation of this extra turn of P1 abolished the formation of P1/P2 hetero-dimer. Systematic truncation studies suggest that P0 contains two spine-helices that each binds one copy of P1/P2 hetero-dimer. Modeling studies suggest that a large hydrophobic cavity, which can accommodate the loop between the spine-helices of P0, can be found on NTD-P1 but not on NTD-P2 when the helix-4 adopts an 'open' conformation. Based on the asymmetric properties of NTD-P1/NTD-P2, a structural model of the eukaryotic P-complex with P2/P1:P1/P2 topology is proposed.

INTRODUCTION

The ribosomal stalk of the large subunit of ribosome is responsible for kingdom-specific binding of translation factors and activation of GTP hydrolysis required for protein synthesis (1,2). The ribosomal stalks from the three domains of life share similarities and differences. They all have a scaffold protein (L10 in bacteria; P0 in eukaryotes and archaea) that has an N-terminal domain for anchoring to the rRNA, and a spine-helix that binds dimers of small ribosomal stalk proteins (L12 in bacteria; P1 in archaea; P1/P2 in eukaryotes). In these small ribosomal stalk proteins, the N-terminal domain is responsible for interacting with the scaffold proteins (L10 or P0) and is connected via a flexible linker to the C-terminal domain responsible for recruiting translation factors (3–6). In bacteria, the stalk consists of ribosomal protein L10 in complex with two or three homo-dimers of L12 (4,7). In the archaeal stalk, acidic ribosomal protein P0 serves as the scaffold protein that binds three copies of homo-dimers of P1 (3). The composition of the eukaryotic stalk is the most complex, consisting of acidic ribosomal proteins P0, P1 and P2 in 1:2:2 ratio (8). Current evidence supports the conclusion that P0 should bind two copies of P1/P2 hetero-dimers, forming a pentameric P-complex of $P0(P1/P2)_2$ (9,10).

Both P1 and P2 exist in free form in the cytoplasm, which are in exchange with those on the ribosome (11). P2 forms a homo-dimer in solution (8,12,13) and its N-terminal domain is responsible for dimerization (10,13,14). We have recently solved the structure of the dimerization domain of P2 homo-dimer and shown that human P2 is homologous to archaeal P1 but structurally distinct from bacterial L12 (15). We also showed that the formation of P1/P2 hetero-dimer is a spontaneous process in which the less stable P2 homo-dimer is displaced by P1 to form a more stable P1/P2 hetero-dimer (15). In the absence of P2, P1 is rapidly degraded in yeast (16).

*To whom correspondence should be addressed. Tel: +852 2609 8004; Fax: +852 2603 5123; Email: kbwong@cuhk.edu.hk

Suppression of P2 expression by RNA interference in human cell lines also leads to the depletion of P1 protein (17). Taken together, it is likely that P1 is protected from degradation by forming a more stable P1/P2 complex.

To provide better understanding on how P1/P2 plays a role in the assembly of eukaryotic stalk, we have determined the structure of the N-terminal dimerization domain of P1/P2 hetero-dimer (NTD-P1/NTD-P2) by nuclear magnetic resonance (NMR) spectroscopy. Although P1 and P2 are homologous to each other, we showed that NTD-P1/NTD-P2 hetero-dimer is structurally asymmetric. The asymmetric properties allowed us to find out the structural element on P1 important for the spontaneous conversion from P2/P2 homo-dimer to P1/P2 hetero-dimer. Based on the structure of NTD-P1/NTD-P2 hetero-dimer, a structural model of human pentameric P-complex was proposed.

MATERIALS AND METHODS

Sample preparation

Preparation of asymmetrically labeled P1/P2 dimerization domain for NMR experiments. DNA fragments corresponding to the N-terminal dimerization domain (NTD) of P1 and P2 (residue 1-69) were cloned into a home-made pRSETA-HisSUMO and pET8c vector, respectively (15). ^{13}C-^{15}N labeled HisSUMO-NTD-P1 and NTD-P2 dimerization domain was expressed in *Escherichia coli* strain C41(DE3) in M9 medium (6 g/l Na_2HPO_4, 3 g/l KH_2PO_4, 0.5 g/l NaCl, 2 mM $MgSO_4$) containing 2 g/l ^{13}C glucose, 1 g/l ^{15}N ammonium chloride and 100 μg/ml ampicllin. Purification of NTD-P1/NTD-P2 hetero-dimer was described previously (15). Protein was concentrated to 1 mM for NMR measurement.

Preparation of P1/P2 and variants for urea-induced denaturation experiments. P1, P1L7A and P1ΔN7 were over-expressed in *E. coli* C41(DE3) strain using LB at 37°C and induced at 0.4 mM IPTG for 4 h before harvesting. Cell lysates of P1, P1L7A and P1ΔN7 were loaded to Q fast flow column pre-equilibrated with 20 mM Tris/HCl, pH 7.8 (buffer A). Proteins collected in flow-through were precipitated by 40% ammonium sulphate. The precipitate was resuspended in 8 M urea, 20 mM Tris/HCl buffer at pH 7.8 and loaded to HiTrap Q HP column pre-equilibrated with the same buffer. Proteins were eluted by a 200 ml gradient of 0–0.5 M NaCl. Urea-denatured P1, P1L7A and P1ΔN7 were refolded by removing urea by dialysis against buffer A. P1 and P1L7A were mixed with P2 [purified as described previously (15)] in 2:1 molar ratio in buffer A. Protein mixtures were incubated at 4°C for 3 h for hetero-dimer formation. Proteins were then concentrated to 5 ml and loaded to HiLoad Superdex 200 gel filtration column equilibrated with 150 mM potassium phosphate pH 7.4. Excess P1 or P1L7A was eluted at void volume and hetero-dimer was eluted at about 200 ml.

Preparation of C-terminal histidine-tagged P2 for pull-down analysis. C-terminal 6 x-histitine-tagged P2 (P2-His thereafter) has similar electrophoretic mobility to P1 in SDS–PAGE, making pull-down assay between P1 and P2-His impossible. To solve this, C-terminal 16× histidine-tagged P2 was cloned by carrying out PCR with reverse primer containing sequence coding for 16 histidines. C-terminal 16× histidine-tagged P2 was over-expressed in *E. coli* C41(DE3) competent cell using LB at 37°C and induced at 0.4 mM IPTG for 4 h before harvesting. Cell lysate of P2-His was loaded to nickel-chelated sepharose equilibrated with buffer B (20 mM PB, 0.5 M NaCl, pH 7.4) containing 40 mM imidazole and eluted using buffer B containing 300 mM imidazole. Imidazole was removed by dialysis before carrying out pull-down assay.

Co-refolding of P0 or its truncation variants with P1/P2. N-terminal His-tagged P0 was expressed as inclusion bodies in *E. coli*. After expression, the inclusion bodies was washed with 0.1% Triton X-100, 0.1% NP-40 in buffer C (1 M NaCl, 20 mM Tris/HCl buffer at pH 7.8), dissolved in 4 M guanidine hydrochloride, and then loaded to a nickel-chelating column pre-equilibrated with 8 M urea in buffer C. His-tagged P0 was eluted by a linear gradient of 0–300 mM imidazole in 8 M urea, buffer C; 10 μM of purified His-tagged P0 was mixed with 30 μM of purified complex of P1/P2. The proteins were denatured in 8 M urea and co-refolded by dialyzing against buffer C. Similar procedures were carried out for other P0 truncation variants (P0ΔC49, P0ΔC86 and P0ΔC120).

Pull-down analysis between P2-His and P1 or P1L7A or P1ΔN7. A total of 100 μg P2-His was mixed with 100 μg P1 or P1L7A or P1ΔN7 and proteins were loaded to nickel-chelated His SpinTrap column (GE Healthcare) pre-equilibrated with buffer B (20 mM PB, 0.5 M NaCl, pH 7.4) containing 40 mM imidazole. After extensive washing, proteins were eluted using buffer B containing 300 mM imidazole. Eluted proteins were then analyzed by SDS–PAGE.

Optimization of buffer condition for NMR spectroscopy by dynamic light scattering. Previous study showed that P1/P2 has a tendency to form high molecular weight oligomer that may hinder NMR analysis (12). To optimize the buffer condition for NMR samples, we have used dynamic light scattering to screen for additives that can avoid aggregation of NTD-P1/NTD-P2 by monitoring the hydrodynamic radius. Different types of additives were tested including salts, chaotropes, amino acids, polysaccharides, protein stabilizer, organic solvents and detergents. Among various additives, CHAPS, which is a non-ionic detergent, is the most effective in avoiding protein aggregation. It was found that the apparent hydrodynamic radius was reduced from 2.5 to 2.1 nm in the presence of 0.3% CHAPS (Supplementary Table S1). As shown in Supplementary Figure S1, addition of 0.3% CHAPS to the sample buffer significantly improved the quality of ^{1}H-^{15}N HSQC spectra. In the subsequent NMR experiments, we dissolved the protein samples in buffer condition containing 0.3% CHAPS, 0.15 M NaCl,

2 mM TCEP, 5 mM DTT, 20 mM sodium phosphate, pH 6.5.

Structure determination of NTD-P1/NTD-P2 by NMR. NMR spectra were collected in Bruker Avance 600 and 700 MHz spectrometers at 298 K. Protein samples of $^{13}C,^{15}N$-NTD-P1/NTD-P2 and NTD-P1/$^{13}C,^{15}N$-NTD-P2 were used to obtain resonance assignment of NTD-P1 and NTD-P2, respectively. Sequential assignment of backbone resonances was obtained by Cα and Cβ connectivities generated by HNCACB and CBCA(CO)NH experiments. Side-chain resonances were obtained from TOCSY-HSQC, H(CC)CONH, HCCH-TOCSY and HCCH-COSY experiments. Inter-proton distance restraints were obtained from NOESY-type experiments such as $^{1}H,^{15}N$-NOESY-HSQC, $^{1}H,^{13}C$-NOESY-HSQC and $^{1}H,^{13}C$-HSQC-NOESY-HSQC. Intermolecular distance restraints were obtained from the ^{13}C-filtered/^{13}C-edited NOESY experiment (18). Chemical shifts were referenced with respect to 4,4-dimethyl-4-silapentane-1-sulfonate. All multidimensional NMR data were processed with NMRPipe (19) and analyzed using NMRView (20). Dihedral angle restraints were derived from TALOS program (21). Hydrogen bond restraints were deduced from deuterium exchange experiments and were only included for those protected amide groups in helices. Structural calculations were performed using ARIA 2.2 (22) and CNS 1.2 (23,24), with an initial set of manually assigned NOEs. The structures converged in the first round of calculation. ARIA-assigned NOEs were checked manually and were included in subsequent rounds of calculation iteratively. Finally, the best 10 structures with the lowest total energy, no NOE and dihedral angle violation were selected. Structural abnormalities in all stages were checked using PROCHECK (25).

Urea-induced denaturation

A total of 0.15 mg/ml protein samples were equilibrated with 0–7.2 M urea in 150 mM potassium phosphate, pH 7.4 for 30 min before CD measurement. Concentration of urea was determined from refractive index measurements (26) using Leica AR200 refractometer. The urea-induced denaturation was monitored by molar ellipticity at 222 nm using a JASCO J810 spectropolarimeter equipped with a peltier-type temperature control unit. The urea-induced denaturation was analyzed as described previously (27). The free energy change of unfolding without denaturant, ΔG_u, was obtained by linear extrapolation model (28): $\Delta G_{(D)} = \Delta G_u - m[D]$, using the average m-value approach (29). ΔG_u of the protein samples were measured at 298 K.

Static light scattering

Protein complexes of 100 µl (P0/P1/P2, P0ΔC49/P1/P2, P0ΔC86/P1/P2 and P0ΔC120/P1/P2) (2–4 mg/ml) were loaded to an analytical gel filtration column Superdex 200 connected to a miniDawn light scattering detector and an Optilab DSP refractometer (Wyatt Technologies). The light scattering data were analysed using the ASTRA software provided by the manufacturer to obtain the molecular mass of the protein complex.

Modeling of human P-complex

To model the structure of human pentameric P0-$(P1/P2)_2$-complex, the structure of human P0 was first modeled by MODELLER (30) using the crystal structure of archaeal *Pyrococcus horikoshii* P0/P1 complex (3) as a template. The structure of human NTD-P1/NTD-P2 was then docked to P0 by superimposition to P1 homo-dimer of archaeal P0/P1 complex. The conformation of helix-4 of NTD-P1/NTD-P2 was modeled by MODELLER. Models of the human P-complex were superimposed to the N-terminal domain of P0 in the crystal structure of yeast 80S ribosome (31). Position of elongation factor 2 was modeled on the crystal structure of yeast 80S ribosome (31) with the aid of previous cryo-EM structure (32).

RESULTS

Overall structure of NTD-P1/NTD-P2 hetero-dimer

It has been shown by us and previous studies that P1 interacts with P2 to form P1/P2 hetero-dimer and their N-terminal domains are responsible for dimerization (10,13–15). To have a better understanding on how they interact with each other, we have determined the solution structure of the N-terminal dimerization domain (NTD) of P1/P2 by NMR and the ensemble of 10 best structures is shown in Figure 1A. Statistics of structural calculation is summarized in Table 1. In NTD-P1/NTD-P2 hetero-dimer, both NTD-P1 and NTD-P2 have four helices in

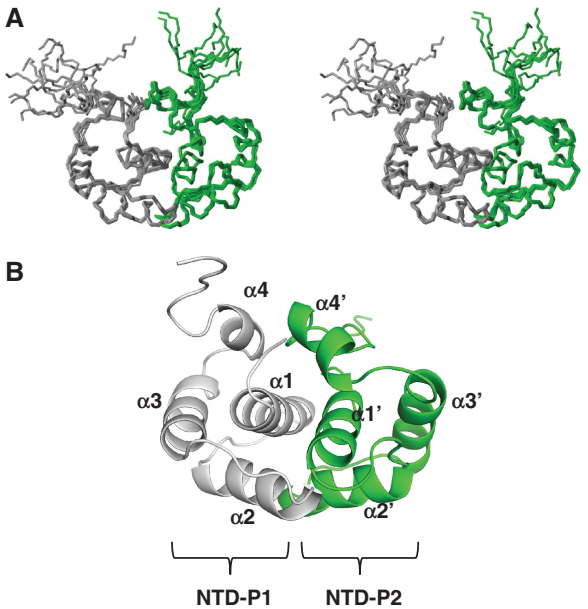

Figure 1. Solution structure of NTD-P1/NTD-P2 hetero-dimer. (**A**) Stereo-diagram of an ensemble of 10 best structures. (**B**) Topology of helices in NTD-P1/NTD-P2 dimerization domain. NTD-P1/NTD-P2 consists of four helices from each chain. Noteworthy, helix-3 is located away from the dimeric interface formed by helices 1, 2 and 4.

Table 1. NMR and refinement statistics for the 10 best structures of NTD-P1/NTD-P2 hetero-dimer

NMR distance and dihedral restraints	
Distance restraints	
Total NOE	4656
Total unambiguous NOE	4355
Intramolecular	4173
Intra-residue	2507
Sequential (|i-j| = 1)	664
Medium-range (|i-j| < 5)	520
Long-range (|i-j| > 4)	482
Intermolecular	182
Total ambiguous NOE	301
Hydrogen bonds	110
Total dihedral angle restraints	
Φ	70
Ψ	70
Structure statistics	
Violations	
Distance restraints[a] (Å)	0.0417 ± 0.0007
Dihedral angle restraint (°)	0.20 ± 0.06
No. of dihedral angle violation > 5°	0
No. of distance restraint violation > 0.5 Å	0
Deviation from idealized geometry	
Bond lengths[a] (Å)	0.0063 ± 0.0001
Bond angles[a] (°)	0.74 ± 0.02
Impropers[a] (°)	1.93 ± 0.09
Average pairwise r.m.s. deviation (Å)	
Heavy[b]	0.731
Backbone[b]	0.316

[a]Values of mean and standard deviation were reported.
[b]r.m.s.d of the structural domain of P1 (residues 1-62) and P2 (residues 1-62) were reported.

which their helices 1, 2 and 4 are facing each other at the dimeric interface. Helices 3 of both NTD-P1 and NTD-P2 are packed away from the interface and are not involved in dimerization (Figure 1B). In this way, their helices 1 are buried inside the core and surrounded by helices 2, 3 and 4.

Dimeric interface of NTD-P1/NTD-P2

Helices 1, 2 and 4 from both NTD-P1 and NTD-P2 form the dimeric interface which buries 1800 A^2 of non-polar and 400 A^2 of polar solvent accessible surface area. The dimeric interface consists of highly conserved residues, i.e. Tyr-11, Leu-14, Ile-15, Leu-31, Ala-34, Ala-35 and Val-37 from NTD-P1 and Ala-5, Leu-8, Leu-9, Ile-26, Val-30 and Ile-55 from NTD-P2 (Figure 2A and B). Helix-1 of both NTD-P1 and NTD-P2 is highly buried, making a number of intermolecular interactions. For example, Leu-9 of NTD-P2 fits nicely into the hydrophobic pocket formed by Ala-8, Tyr-11, Ile-15, Leu-31, Ile-32, Ala-35 and Val-37, forming extensive intermolecular hydrophobic interactions (Figure 2A). These interactions are supported by intermolecular NOEs observed (Figure 2C).

Structural comparison between NTD-P1/NTD-P2 and NTD-P2/NTD-P2

The topology of human NTD-P1/NTD-P2 hetero-dimer and NTD-P2 homo-dimer are similar (Figure 3A). Each monomer of NTD-P1 or NTD-P2 consists of four helices, with helix-1 buried in a hydrophobic core and helix-3 packed away from the dimeric interface. Unlike the symmetric NTD-P2 homo-dimer, the structure of NTD-P1/NTD-P2 hetero-dimer is asymmetric. First, there are three conserved charged residues (Asp-37, Arg-38 and Lys-41) (Figure 2B) that are exposed on the helix-3 of NTD-P2. These charged residues are substituted by conserved hydrophobic residues (Phe-42, Trp-43 and Leu-46) in NTD-P1 (Figure 3A). Second, NTD-P1 and NTD-P2 differ in their orientation of helix-4 (Figure 3A). In NTD-P2 homo-dimer, helix-4 packs on helix-1 of the same chain (Figure 3A). In contrast, in NTD-P1/NTD-P2 hetero-dimer, helix-4 of NTD-P2 packs on helix-1 of the NTD-P1 (Figure 3A). Such packing is facilitated by NTD-P1 having a longer helix-1, in which the extra turn allows Leu-7 of NTD-P1 to form hydrophobic interaction with Glu-52, Ile-55 and Ala-56 of NTD-P2 (Figure 3B). On the other hand, helix-4 of NTD-P1 is packed on a hydrophobic cleft formed by helix-1 and -3 of NTD-P1 (Figure 3C). This cleft is only present in NTD-P1 due to the differences in packing of helix-1 and -3 in NTD-P1 and NTD-P2. Helix-1 packs on helix-3 at an angle of approximately 30° in NTD-P1, but at an angle of approximately −60° in NTD-P2 (Figure 3D).

The extra turn of helix-1 of P1 is important for P1/P2 dimerization

P2 forms a homo-dimer in solution (8,12,13). However, addition of P1 to P2/P2 homo-dimer causes spontaneous conversion, forming a more stable P1/P2 hetero-dimer (15). Structural comparison of the dimerization domains of P1/P2 and P2/P2 showed that helix-1 of P1 has a longer helix-1, in which the extra turn forms extensive inter-molecular interactions with helix-1 and -4 of P2 (Figure 3B). Therefore, we hypothesized that the extra turn on helix-1 of P1 is important for P1/P2 dimerization. To test this hypothesis, the extra turn was truncated (P1ΔN7) and the interaction with P2 was investigated by pull-down analysis. Histidine-tagged P2 was mixed with either P1 or P1ΔN7 and then loaded to nickel-chelated sepharose (Figure 4A, lanes 1 and 3). After extensive washing, P2 was found to be co-eluted with wild-type P1 but not with P1ΔN7 (Figure 4A, lanes 2 and 4). Our observation showed that the extra turn on helix-1 of P1 is a structural element important for P1/P2 hetero-dimer formation.

Next, we investigated why the extra-turn is essential to P1/P2 formation. We noticed that Leu-7 at the extra turn of P1 forms inter-molecular interaction with Leu-12, Glu-52, Ile-55 and Ala-56 of P2 (Figure 3B). We hypothesized that these extra inter-molecular interactions stabilize P1/P2 hetero-dimer. To test this hypothesis, we created an L7A variant of P1 (P1L7A) and performed urea-induced denaturation experiment to measure the conformational stability of P1/P2, P1L7A/P2 and P2/P2. Denaturation of wild-type P1/P2 resembled a two-state transition with a mid-point of transition ($[D]_{1/2}$) of 3.8 ± 0.3 M and free energy of unfolding (ΔG_u) of 13.2 ± 2.0 kJ/mol. The stability of P1L7A/P2 was lower

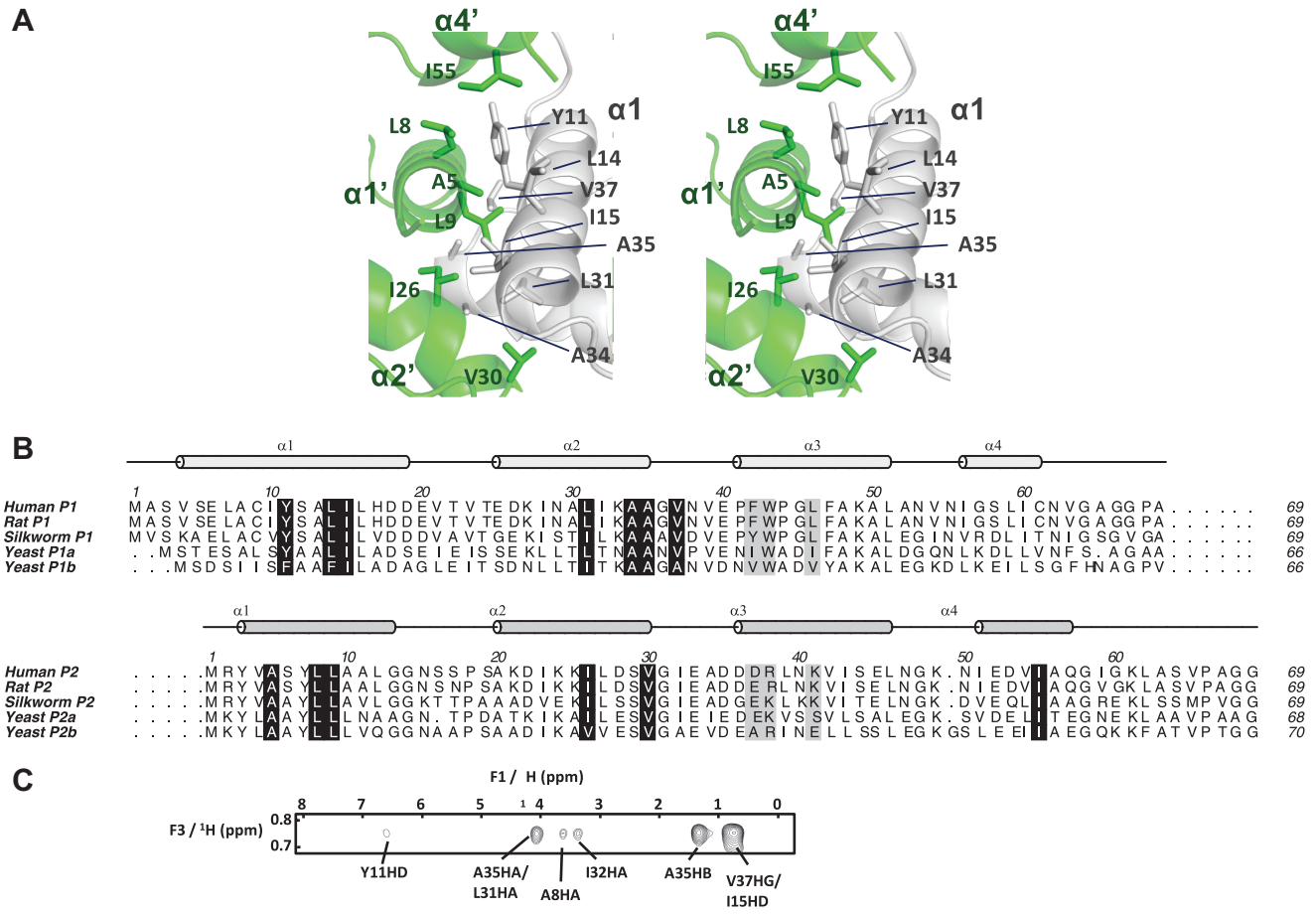

Figure 2. Dimeric interface of NTD-P1/NTD-P2. (A) Stereo-diagram showing the close-up view of the dimeric interface. NTD-P1 and NTD-P2 are colored coded gray and green, respectively. (**B**) Sequence alignment of NTD-P1 and NTD-P2. Conserved residues in the dimeric interface are shaded black. Conserved hydrophobic residues (shaded gray) on helix-3 of P1 are substituted by charged residues on P2. (**C**) Intermolecular NOEs were obtained from the three dimensional ^{13}C F1 -filtered, F3 -edited NOESY-HSQC experiment (18) acquired on an asymmetrically labeled NTD-P1/NTD-P2 sample. A selected F1-F3 plane at ^{13}C frequency (26.5 ppm) of NTD-P2 L9 CD1 was shown.

than that of wild-type P1/P2, with values $[D]_{1/2}$ and $\Delta G_{\text{unfolding}}$ of 2.4 ± 0.4 M and 8.3 ± 1.8 kJ/mol, respectively (Figure 4B). These results suggest that Leu-7 of P1 forms extra inter-molecular interactions to stabilize P1/P2 hetero-dimer. Noteworthy, P2/P2 homo-dimer was less stable than both P1/P2 and P1L7A/P2 hetero-dimer (Figure 4B), which explains why P2 can form hetero-dimer with both P1 and P1L7A (Supplementary Figure S2). Taken together, spontaneous hetero-dimer formation of P1/P2 is driven by thermodynamics stability, which is provided by the extra interactions from the first-turn of helix-1 of P1.

C-terminal domain of P0 contains two separate binding regions that each binds one copy of P1/P2 hetero-dimer

It was found that the C-terminal domain of archaeal P0 has three spine-helices, and each spine-helix binds one copy of P1/P1 homo-dimer (3). We have previously demonstrated that P0 can bind two P1/P2 hetero-dimers to form an 80 kDa pentameric complex (15). Sequence alignment and secondary structure prediction suggest that the C-terminal domain of human P0 has two spine-helices (Figure 5A). We hypothesized that each of the spine-helices binds one copy of P1/P2 hetero-dimer. To test this hypothesis, we have created three truncation variants of P0, in which the flexible tail (P0ΔC49), together with one spine-helix (P0ΔC86) or two spine-helices (P0ΔC120) were removed. P0 or its truncation variants were co-refolded with P1 and P2, and the molecular mass of the co-refolded complex was analyzed by static light scattering (Figure 5B). For P0 and P0ΔC49, single peak of 79.8 and 76.0 kDa, respectively, were eluted, showing that both P0 and P0ΔC49 can interact with two P1/P2 hetero-dimers to form a pentameric complex. For P0ΔC86, the peak of 47.9 kDa is consistent with the molecular weight for a trimeric complex, in which P0ΔC86 binds one copy of P1/P2 hetero-dimer, while the peak of 23.3 kDa corresponds to the excess hetero-dimer of P1/P2 (Figure 5B). In contrast, P0ΔC120 cannot form complex with P1/P2 and was aggregated. Our results showed that the C-terminal tail of human P0 (residue 269–317) is not responsible for the formation of the pentameric P-complex

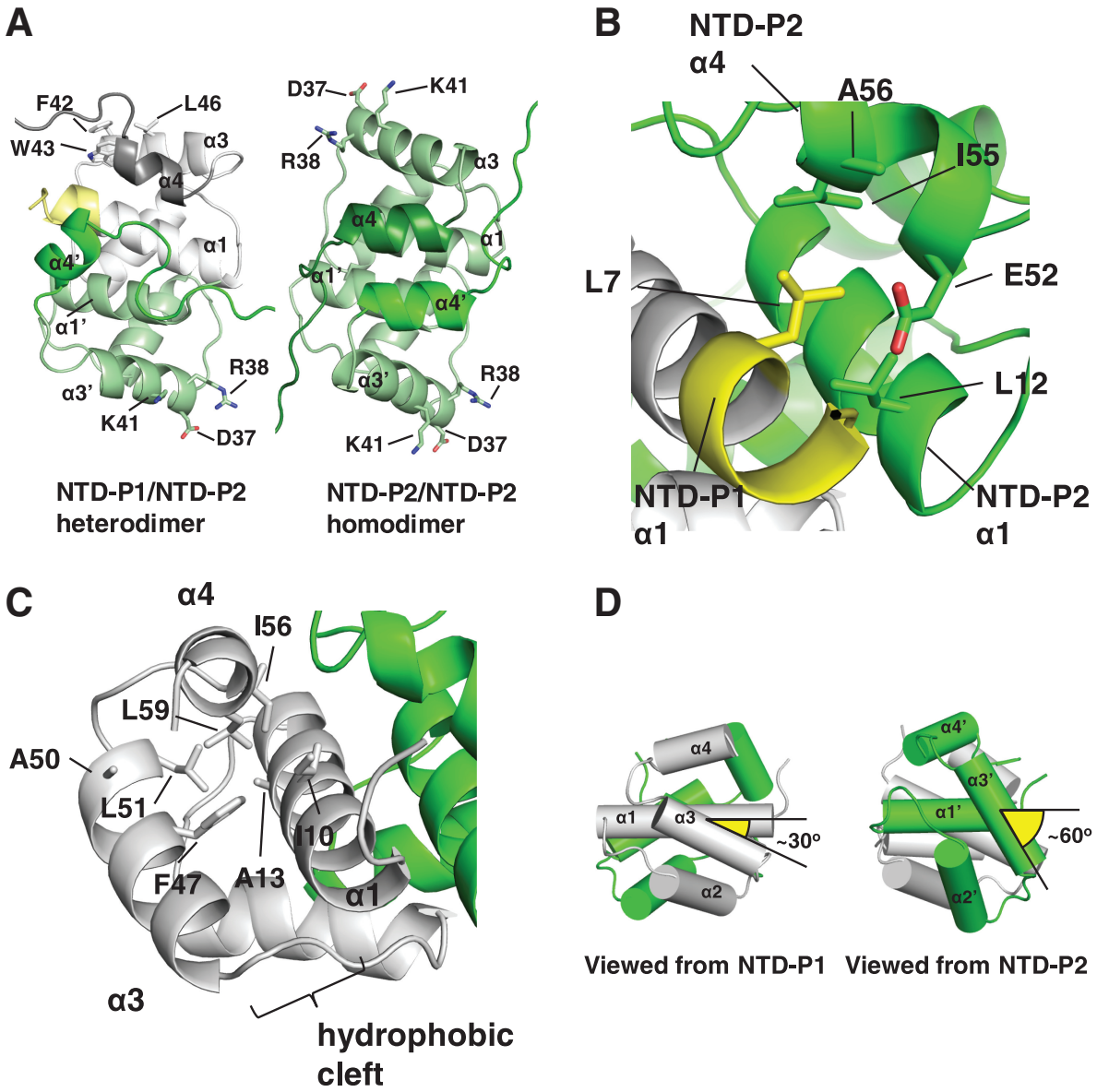

Figure 3. The structure of NTD-P1/NTD-P2 is asymmetric. (**A**) Structural comparison between NTD-P1/NTD-P2 hetero-dimer and NTD-P2 homo-dimer. Three conserved charged residues (Asp-37, Arg-38 and Lys-41) that are exposed on the helix-3 of NTD-P2 are substituted by conserved hydrophobic residues (Phe-42, Trp-43 and Leu-46) in NTD-P1. Moreover, helix-4 of NTD-P2 homo-dimer packs on helix-1 of the same chain while helix-4 of NTD-P2 packs on helix-1 of the NTD-P1 in the case of NTD-P1/NTD-P2. (**B**) Helix 1 of NTD-P1 has an extra turn (yellow). The extra turn of NTD-P1 helix-1 allows Leu-7 to form hydrophobic interaction with Leu-12, Glu-52, Ile-55 and Ala-56 of NTD-P2. (**C**) Packing of NTD-P1 helix-4. Helix-4 of NTD-P1 packs on a hydrophobic cleft formed by helix-1 and 3 of NTD-P1. Hydrophobic residues along the cleft are indicated. (**D**) The inter-helical angles between helix-1 and 3 are different in NTD-P1 (gray) and NTD-P2 (green).

and identified two binding sites (197–231 and 232–268) that each binds one copy of P1/P2 hetero-dimer.

DISCUSSION

Eukaryotic, archaeal and bacterial stalks have different structural composition (5,6). The structures of bacterial and archaeal stalk complex were determined previously (3,4). However, structural information about eukaryotic ribosomal stalk proteins is scarce, probably due to intrinsic flexibility of the stalk proteins. For example, the structures of P1 and P2 are lacking in the crystal structure of yeast ribosome recently solved (31). To provide a better understanding of the structure-function of eukaryotic ribosomal stalk, we have determined the structure of the dimerization domain of P1/P2 hetero-dimer (NTD-P1/NTD-P2) by NMR spectroscopy.

Structural comparison reveals that the extra-turn of helix-1 of P1 forms many intermolecular interactions with helix-1 and -4 of P2. Truncation of this extra turn abolished the formation of P1/P2 hetero-dimer (Figure 4A). This suggests that the extra turn on P1 play a vital role in stabilizing P1/P2 hetero-dimer and explains

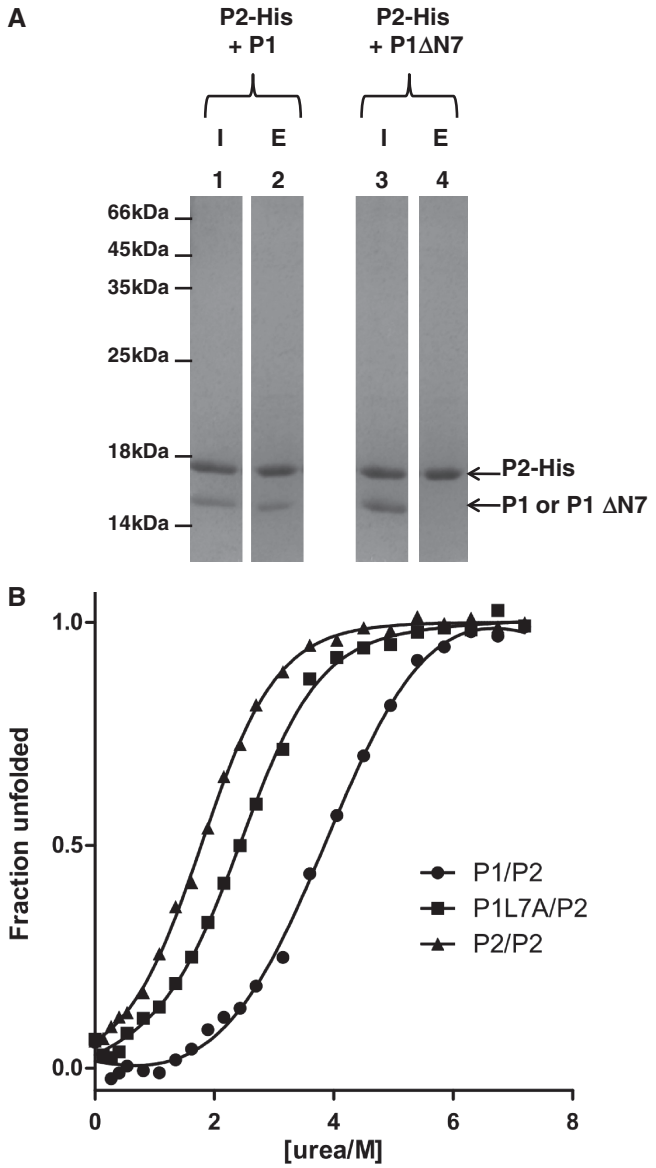

Figure 4. First turn of helix-1 of P1 is important for P1/P2 dimerization. (**A**) Pull-down assay showing that extra turn on P1 is an important structural element for the formation of stable P1/P2 hetero-dimer. Histidine-tagged P2 was mixed with either P1 or P1ΔN7 and then loaded to nickel chelated sepharose (lanes 1 and 3, labeled as 'I'). After extensive washing, P2-His was found co-eluted with P1 but not P1ΔN7 (lanes 2 and 4, labeled as 'E'), showing that P2 interact with P1 but not with P1ΔN7. (**B**) Leu-7 located at the first turn of helix-1 of P1 contributes to the stability of P1/P2 hetero-dimer. Conformational stability of P2 homo-dimer, P1/P2 and P1L7A/P2 hetero-dimer was determined by urea-induced denaturation experiment. Mid-point of transition and the free energy of unfolding were 1.8 ± 0.2 M and 6.8 ± 1.0 kJ/mol for P2 homo-dimer, 2.4 ± 0.4 M and 8.3 ± 1.8 kJ/mol for P1L7A/P2 and 3.8 ± 0.3 M and 13.2 ± 2.0 kJ/mol for P1/P2 hetero-dimer.

the spontaneous conversion from P2/P2 homo-dimer to P1/P2 hetero-dimer. Moreover, P2/P2 homo-dimer cannot interact with P0 (9,10,15,33) and pre-formed P0/P1 complex (9,10,34). Taken together, it is likely that P1 and P2 form a hetero-dimer, which then bind to P0 to assemble the pentameric P-complex.

The structure of human NTD-P1/NTD-P2 is very different from the structure of bacterial L12 homo-dimer (Supplementary Figure S3) (4,35,36). On the other hand, the structures of human NTD-P1/NTD-P2 and archaeal NTD-P1 homo-dimer (3) are homologous to each other. The most notable structural differences are in helix-4. In the crystal structure of archaeal stalk complex P0(P1/P1)$_3$, helix-4 of NTD-P1 adopts an 'open' conformation, which exposes the hydrophobic residues on helix-1 and helix-3 and allows the binding of P0 spine-helix (3). In contrast, the helix-4 adopts a 'closed' conformation in human NTD-P1/NTD-P2 hetero-dimer. It was found that archaeal stalk complex can render *E. coli* ribosome accessible to eukaryotic elongation factors at levels comparable to eukaryotic stalk complex (37). This result indicates that the ribosomal stalks are functionally conserved between eukaryotic and archaeal organisms. Moreover, when we compared the structure of human NTD-P1/NTD-P2 hetero-dimer with that of NTD-P2 homo-dimer (15), we noticed differences in the orientation of helix-4 in these structures (Figure 3). This observation suggests that helices 4 in NTD-P1 and NTD-P2 are versatile and able to adopt different conformations. Taken together, it is very likely that in eukaryotic stalk complex P0(P1/P2)$_2$, helix-4 of P1/P2 may adopt an 'open' conformation similar to that observed in archaeal stalk complex and facilitate binding of P0 spine-helices.

The structural composition of the eukaryotic stalk is more complex than archaeal stalk. Unlike the archaeal stalk in which P0 binds three homo-dimers of P1 (3), the eukaryotic stalk involves the association of two copies of P1/P2 hetero-dimers to P0. Previous studies on silkworm and yeast P0 suggested that P0 has two binding sites for P1/P2 hetero-dimer (38,39). Sequence analyses predicted that human P0 has two spine-helices next to the RNA-binding domain. In our study, we further showed that each spine-helix bind one copy of P1/P2 hetero-dimers (Figure 5). Unlike archaeal P0 that binds homo-dimers of P1, eukaryotic P0 binds hetero-dimers of P1/P2. Because of the asymmetry of P1/P2 hetero-dimer, there could be two orientations of how P1/P2 binds to a P0 spine-helix. As a result, there will be four possible topological arrangements of P1/P2 in P0(P1/P2)$_2$, namely P1/P2:P1/P2, P1/P2:P2/P1, P2/P1:P2/P1 and P2/P1:P1/P2. For example, in the case of P2/P1:P1/P2, P2 occupies positions 1 and 4, while P1 occupies positions 2 and 3 of the two spine-helices (Figure 6A).

Our structure of NTD-P1/NTD-P2 strongly favors the topology of P2/P1:P1/P2. Because the P-proteins located at position 2 and 3 need to accommodate the P0 loop between the two spine-helices, it should be different from the P-proteins located at positions 1 and 4 (Figure 6A). The P0 loop is bulky because it contains a conserved Tyr-Pro motif, which consists of a large hydrophobic residue (Tyr/Phe/Ile) and a proline residue (Supplementary Figure S4A). In Figure 6B, we modeled the exposed hydrophobic surface on the dimerization domain of P1/P2 after the helix-4 adopts an 'open' conformation. We noticed that a hydrophobic cavity can be

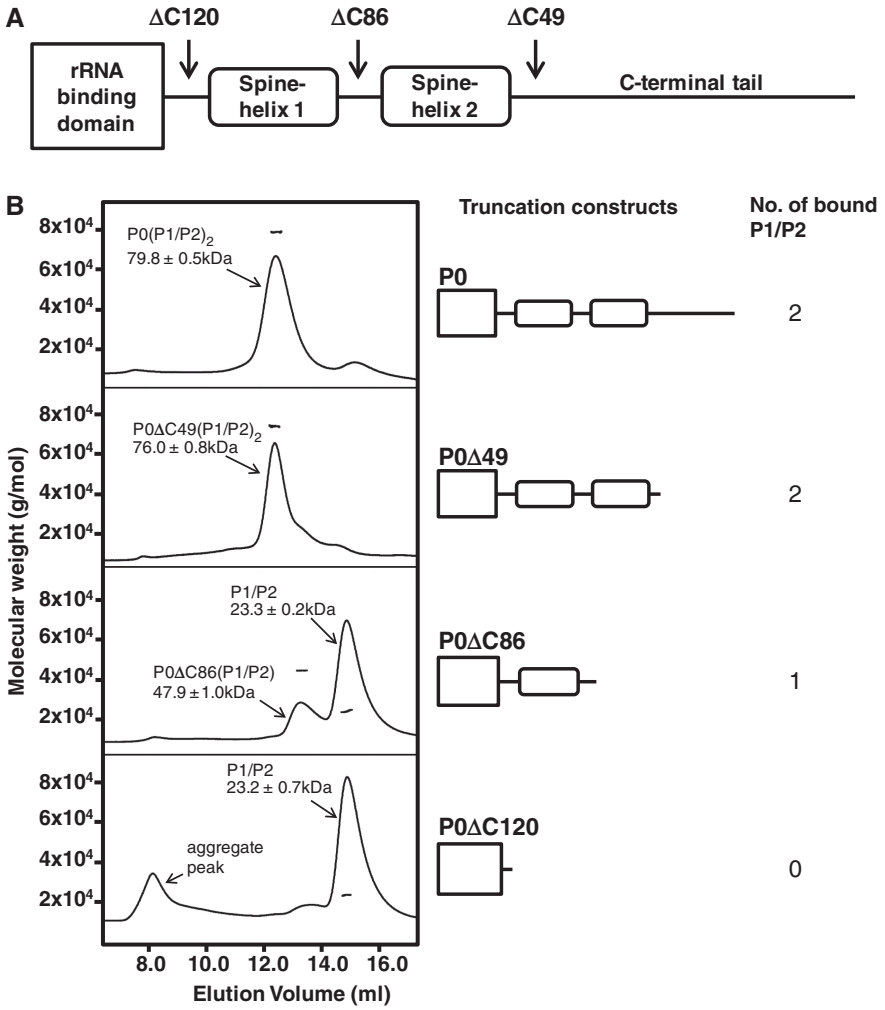

Figure 5. C-terminal domain of P0 has separate regions for binding two P1/P2 hetero-dimers. (**A**) C-terminal domain of human P0 was predicted to have two spine-helices. Arrows indicates the position where truncation was made. (**B**) Determination of the number of P1/P2 bound to P0 or its truncation variants. P0 or its truncation variants were co-refolded with P1/P2 hetero-dimer and the molecular mass of the co-refolded proteins were analyzed by static light scattering. For P0 and P0ΔC49, single peak of 79.8 kDa and 76.0 kDa respectively were eluted, showing that both P0 (34.3 kDa) and P0ΔC49 (29.5 kDa) can interact with two P1/P2 hetero-dimers (23.2 kDa) to form a pentameric complex (expected MW for pentameric $P0(P1/P2)_2$ and $P0\Delta C49(P1/P2)_2$ are 80.7 kDa and 75.9 kDa, respectively). For P0ΔC86, two peaks of 47.9 kDa and 23.3 kDa were eluted, showing that P0ΔC86 (25.5 kDa) can only interact with one P1/P2 hetero-dimer (expected MW for trimeric P0ΔC86(P1/P2) is 48.7 kDa) and the excess P1/P2 was eluted after the trimer peak. For P0ΔC120, there is a peak at void volume and a peak of 23.2 kDa. This showed that P0ΔC120 (21.6 kDa) form high molecular weight aggregate and cannot form complex with P1/P2. Free P1/P2 was then eluted as a hetero-dimer.

found on NTD-P1 side but not on NTD-P2 side (Figure 6B). It is likely that this cavity on P1 is responsible for accommodating the bulky P0 loop between the two spine-helices. As shown in Figure 6C, the P2/P1:P1/P2 topology brings two P1 together and forms a large hydrophobic cavity that can accommodate the P0 loop (Figure 6C). Based on the P2/P1:P1/P2 topology, we constructed a structural model of human P-complex (Supplementary Figure S4B). This model is consistent with a previous fluorescence study on yeast P-complex, which showed that a conserved tryptophan residue (Trp-40 in yeast, Trp-43 in human) on helix-3 of P1 become buried upon formation of the P-complex (40). In our model, the conserved hydrophobic residues (Phe-42, Trp-43 and Leu-46) of helix-3 of P1 make extensive hydrophobic interactions with each other (Supplementary Figure S4B). As pointed out previously by our group (15), these conserved hydrophobic residues of P1 are replaced by charged residues in P2 (Figure 3A). We showed that substitutions of these conserved hydrophobic residues in P1 with charged residues abolish the formation of P-complex (15). Our model can also explain a previous observation that the pentameric complex $P0(P1/P2)_2$ was >2-fold more stable than the trimeric complex P0(P1/P2) (40). Presumably, the hydrophobic interactions between P1 and the P0 loop cooperatively stabilize the pentameric P-complex. Other topological arrangements (P2/P1:P2/P1, P1/P2:P2/P1 and P1/P2:P1/P2) involve unfavorable burial of these charged residues, and thus, are unlikely.

The crystal structure of yeast ribosome was recently solved (31). However, only the N-terminal RNA binding

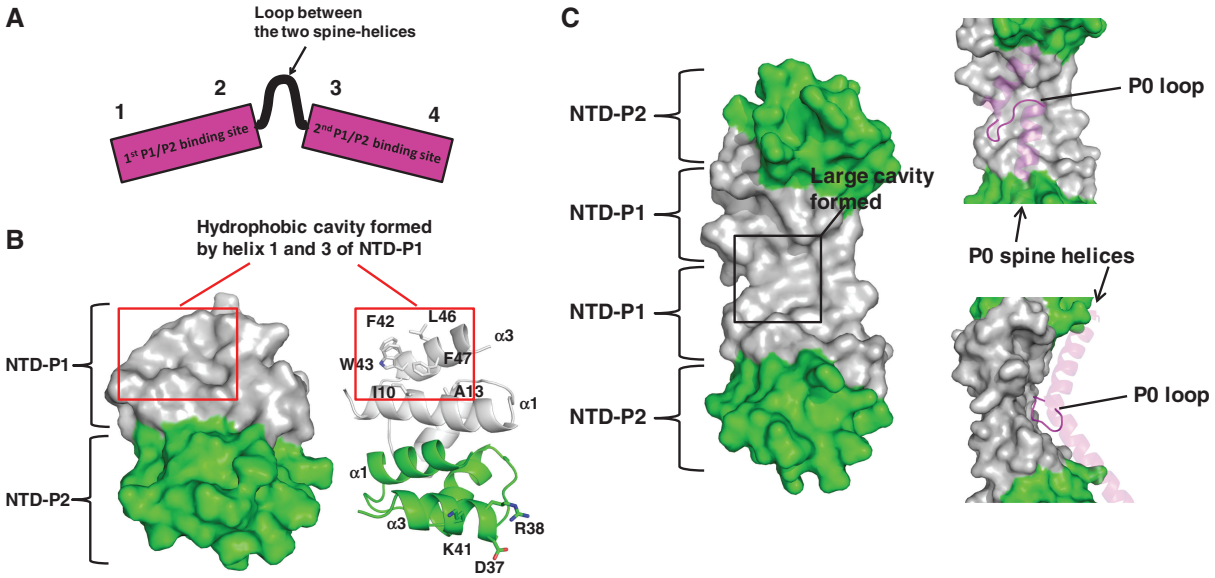

Figure 6. Asymmetric structure of NTD-P1/NTD-P2 suggests that eukaryotic P-complex adopts a P2/P1:P1/P2 topology. (**A**) Schematic diagram showing that there are four small P-protein binding sites on P0. The two spine-helices of P0 (magenta box) are connected by a loop. Each spine-helix has two P-protein binding sites. P-proteins that bind at position 2 and 3 are expected to interact with the connecting P0 loop. (**B**) A model of exposed surface of NTD-P1/NTD-P2 when the helix-4 adopts an 'open' conformation. A hydrophobic cavity is present on the NTD-P1 side (gray) but not the NTD-P2 side (green). Exposed hydrophobic residues of NTD-P1 are indicated. (C) The P2/P1:P1/P2 topology creates a large hydrophobic cavity for binding the P0 loop between the spine-helices.

domain of P0 is visible, and the structure lacks electron density for P1 and P2 (31). Guided by the location of the N-terminal RNA binding domain of P0, we dock our model of human P-complex to the crystal structure of the yeast ribosome (Supplementary Figure S5). Multiple copies of the C-terminal tails of P-proteins are extending from the dimerization domain, and they can provide more binding sites for translation factors, and thus, increase local factor concentration, leading to a more efficient recruitment of translation factors (4,41). In eukaryotic stalk protein, there is a highly conserved SDDDMGFGLFD motif at the C-terminus, which is responsible for binding elongation factors (42,43) and ribosome-inactivating proteins (44–46). Since both ribosome-inactivating proteins and elongation factors bind to the sarcin-ricin loop of 28 S rRNA, our structural model of human P-complex suggests that the flexible C-terminal tails protruding from the extended stalk region can physically reach the binding site for elongation factors and ribosome-inactivating proteins. It is likely that the conserved C-terminal tails in eukaryotic stalk serve a role in fetching the translation factors and ribosome-inactivating proteins in the cytoplasm, and recruiting them to the ribosome.

ACCESSION NUMBERS

Atomic coordinates for the refined structures have been deposited with the Protein Data Bank under accession code 2LBF. Chemical shifts and restraints have been deposited with the Biological Magnetic Resonance Bank under accession number 17557. PDB accession number 2LBF.

SUPPLEMENTARY DATA

Supplementary Data are available at NAR Online: Supplementary Table 1, Supplementary Figures 1–5, Supplementary References [31–32].

ACKNOWLEDGEMENTS

Figure 1A was produced by MOLMOL and other molecular images were produced by PyMOL.

FUNDING

General Research Fund (Project no. 477509) from the Research Grants Council of Hong Kong SAR; Special Equipment Grants (Project no. SEG/CUHK09) from the University Grants Committee of Hong Kong SAR. The funders had no role in study design, data collection and analysis, decision to publish or preparation of the manuscript. Funding for open access charge: The Chinese University of Hong Kong.

Conflict of interest statement. None declared.

REFERENCES

1. Uchiumi,T., Honma,S., Nomura,T., Dabbs,E.R. and Hachimori,A. (2002) Translation elongation by a hybrid ribosome in which proteins at the GTPase center of the *Escherichia coli* ribosome are replaced with rat counterparts. *J. Biol. Chem.*, **277**, 3857–3862.
2. Uchiumi,T., Hori,K., Nomura,T. and Hachimori,A. (1999) Replacement of L7/L12.L10 protein complex in Escherichia coli ribosomes with the eukaryotic counterpart changes the specificity of elongation factor binding. *J. Biol. Chem.*, **274**, 27578–27582.

3. Naganuma,T., Nomura,N., Yao,M., Mochizuki,M., Uchiumi,T. and Tanaka,I. (2010) Structural basis for translation factor recruitment to the eukaryotic/archaeal ribosomes. *J. Biol. Chem.*, **285**, 4747–4756.
4. Diaconu,M., Kothe,U., Schlunzen,F., Fischer,N., Harms,J.M., Tonevitsky,A.G., Stark,H., Rodnina,M.V. and Wahl,M.C. (2005) Structural basis for the function of the ribosomal L7/12 stalk in factor binding and GTPase activation. *Cell*, **121**, 991–1004.
5. Gonzalo,P. and Reboud,J.P. (2003) The puzzling lateral flexible stalk of the ribosome. *Biol. Cell*, **95**, 179–193.
6. Wahl,M.C. and Moller,W. (2002) Structure and function of the acidic ribosomal stalk proteins. *Curr. Prot. Pept. Sci.*, **3**, 93–106.
7. Pettersson,I., Hardy,S.J. and Liljas,A. (1976) The ribosomal protein L8 is a complex L7/L12 and L10. *FEBS Lett.*, **64**, 135–138.
8. Uchiumi,T., Wahba,A.J. and Traut,R.R. (1987) Topography and stoichiometry of acidic proteins in large ribosomal subunits from Artemia salina as determined by crosslinking. *Proc. Natl Acad. Sci. USA*, **84**, 5580–5584.
9. Shimizu,T., Nakagaki,M., Nishi,Y., Kobayashi,Y., Hachimori,A. and Uchiumi,T. (2002) Interaction among silkworm ribosomal proteins P1, P2 and P0 required for functional protein binding to the GTPase-associated domain of 28S rRNA. *Nucleic Acids Res.*, **30**, 2620–2627.
10. Gonzalo,P., Lavergne,J.P. and Reboud,J.P. (2001) Pivotal role of the P1 N-terminal domain in the assembly of the mammalian ribosomal stalk and in the proteosynthetic activity. *J. Biol. Chem.*, **276**, 19762–19769.
11. Zinker,S. and Warner,J.R. (1976) The ribosomal proteins of *Saccharomyces cerevisiae*. Phosphorylated and exchangeable proteins. *J. Biol. Chem.*, **251**, 1799–1807.
12. Grela,P., Sawa-Makarska,J., Gordiyenko,Y., Robinson,C.V., Grankowski,N. and Tchorzewski,M. (2008) Structural properties of the human acidic ribosomal P proteins forming the P1-P2 heterocomplex. *J. Biochem.*, **143**, 169–177.
13. Tchorzewski,M., Boguszewska,A., Dukowski,P. and Grankowski,N. (2000) Oligomerization properties of the acidic ribosomal P-proteins from *Saccharomyces cerevisiae*: effect of P1A protein phosphorylation on the formation of the P1A-P2B hetero-complex. *Biochim. Biophys. Acta*, **1499**, 63–73.
14. Naganuma,T., Shiogama,K. and Uchiumi,T. (2007) The N-terminal regions of eukaryotic acidic phosphoproteins P1 and P2 are crucial for heterodimerization and assembly into the ribosomal GTPase-associated center. *Genes Cells*, **12**, 501–510.
15. Lee,K.M., Yu,C.W., Chan,D.S., Chiu,T.Y., Zhu,G., Sze,K.H., Shaw,P.C. and Wong,K.B. (2010) Solution structure of the dimerization domain of ribosomal protein P2 provides insights for the structural organization of eukaryotic stalk. *Nucleic Acids Res.*, **38**, 5206–5216.
16. Nusspaumer,G., Remacha,M. and Ballesta,J.P. (2000) Phosphorylation and N-terminal region of yeast ribosomal protein P1 mediate its degradation, which is prevented by protein P2. *EMBO J.*, **19**, 6075–6084.
17. Martinez-Azorin,F., Remacha,M. and Ballesta,J.P. (2008) Functional characterization of ribosomal P1/P2 proteins in human cells. *Biochem. J.*, **413**, 527–534.
18. Zwahlen,C., Legault,P., Vincent,S.J.F., Greenblatt,J., Konrat,R. and Kay,L.E. (1997) Methods for measurement of intermolecular NOEs by multinuclear NMR spectroscopy: Application to a bacteriophage lambda N-peptide/boxB RNA complex. *J. Am. Chem. Soc.*, **119**, 6711–6721.
19. Delaglio,F., Grzesiek,S., Vuister,G.W., Zhu,G., Pfeifer,J. and Bax,A. (1995) NMRPipe: a multidimensional spectral processing system based on UNIX pipes. *J. Biomol. NMR*, **6**, 277–293.
20. Johnson,B.A. and Blevins,R.A. (1994) NMRView: a computer program for the visualization and analysis of NMR data. *J. Biomol. NMR*, **4**, 603–614.
21. Cornilescu,G., Delaglio,F. and Bax,A. (1999) Protein backbone angle restraints from searching a database for chemical shift and sequence homology. *J. Biomol. NMR*, **13**, 289–302.
22. Linge,J.P., O'Donoghue,S.I. and Nilges,M. (2001) Automated assignment of ambiguous nuclear overhauser effects with ARIA. *Methods Enzymol.*, **339**, 71–90.
23. Brunger,A.T. (2007) Version 1.2 of the Crystallography and NMR system. *Nat. Protoc.*, **2**, 2728–2733.
24. Brunger,A.T., Adams,P.D., Clore,G.M., DeLano,W.L., Gros,P., Grosse-Kunstleve,R.W., Jiang,J.S., Kuszewski,J., Nilges,M., Pannu,N.S. *et al.* (1998) Crystallography & NMR system: A new software suite for macromolecular structure determination. *Acta Cryst.*, **D54**, 905–921.
25. Laskowski,R.A., Rullmannn,J.A., MacArthur,M.W., Kaptein,R. and Thornton,J.M. (1996) AQUA and PROCHECK-NMR: programs for checking the quality of protein structures solved by NMR. *J. Biomol. NMR*, **8**, 477–486.
26. Pace,C.N. (1986) Determination and analysis of urea and guanidine hydrochloride denaturation curves. *Methods Enzymol.*, **131**, 266–280.
27. Chan,C.H., Yu,T.H. and Wong,K.B. Stabilizing salt-bridge enhances protein thermostability by reducing the heat capacity change of unfolding. *PLoS One*, **6**, e21624.
28. Santoro,M.M. and Bolen,D.W. (1988) Unfolding free energy changes determined by the linear extrapolation method. 1. Unfolding of phenylmethanesulfonyl alpha-chymotrypsin using different denaturants. *Biochemistry*, **27**, 8063–8068.
29. Itzhaki,L.S., Otzen,D.E. and Fersht,A.R. (1995) The structure of the transition state for folding of chymotrypsin inhibitor 2 analysed by protein engineering methods: evidence for a nucleation-condensation mechanism for protein folding. *J. Mol. Biol.*, **254**, 260–288.
30. Marti-Renom,M.A., Stuart,A.C., Fiser,A., Sanchez,R., Melo,F. and Sali,A. (2000) Comparative protein structure modeling of genes and genomes. *Annu. Rev. Biophys. Biomol. Struct.*, **29**, 291–325.
31. Ben-Shem,A., Jenner,L., Yusupova,G. and Yusupov,M. (2010) Crystal structure of the eukaryotic ribosome. *Science*, **330**, 1203–1209.
32. Spahn,C.M., Gomez-Lorenzo,M.G., Grassucci,R.A., Jorgensen,R., Andersen,G.R., Beckmann,R., Penczek,P.A., Ballesta,J.P. and Frank,J. (2004) Domain movements of elongation factor eEF2 and the eukaryotic 80S ribosome facilitate tRNA translocation. *EMBO J.*, **23**, 1008–1019.
33. Zurdo,J., Parada,P., van den Berg,A., Nusspaumer,G., Jimenez-Diaz,A., Remacha,M. and Ballesta,J.P. (2000) Assembly of Saccharomyces cerevisiae ribosomal stalk: binding of P1 proteins is required for the interaction of P2 proteins. *Biochemistry*, **39**, 8929–8934.
34. Krokowski,D., Tchorzewski,M., Boguszewska,A. and Grankowski,N. (2005) Acquisition of a stable structure by yeast ribosomal P0 protein requires binding of P1A-P2B complex: in vitro formation of the stalk structure. *Biochim. Biophys. Acta*, **1724**, 59–70.
35. Bocharov,E.V., Sobol,A.G., Pavlov,K.V., Korzhnev,D.M., Jaravine,V.A., Gudkov,A.T. and Arseniev,A.S. (2004) From structure and dynamics of protein L7/L12 to molecular switching in ribosome. *J. Biol. Chem.*, **279**, 17697–17706.
36. Wahl,M.C., Bourenkov,G.P., Bartunik,H.D. and Huber,R. (2000) Flexibility, conformational diversity and two dimerization modes in complexes of ribosomal protein L12. *EMBO J.*, **19**, 174–186.
37. Nomura,T., Nakano,K., Maki,Y., Naganuma,T., Nakashima,T., Tanaka,I., Kimura,M., Hachimori,A. and Uchiumi,T. (2006) In vitro reconstitution of the GTPase-associated centre of the archaebacterial ribosome: the functional features observed in a hybrid form with Escherichia coli 50S subunits. *Biochem. J.*, **396**, 565–571.
38. Krokowski,D., Boguszewska,A., Abramczyk,D., Liljas,A., Tchorzewski,M. and Grankowski,N. (2006) Yeast ribosomal P0 protein has two separate binding sites for P1/P2 proteins. *Mol. Microbiol.*, **60**, 386–400.
39. Hagiya,A., Naganuma,T., Maki,Y., Ohta,J., Tohkairin,Y., Shimizu,T., Nomura,T., Hachimori,A. and Uchiumi,T. (2005) A mode of assembly of P0, P1, and P2 proteins at the GTPase-associated center in animal ribosome: in vitro analyses with P0 truncation mutants. *J. Biol. Chem.*, **280**, 39193–39199.
40. Grela,P., Krokowski,D., Gordiyenko,Y., Krowarsch,D., Robinson,C.V., Otlewski,J., Grankowski,N. and Tchorzewski,M.

(2010) Biophysical properties of the eukaryotic ribosomal stalk. *Biochemistry*, **49**, 924–933.
41. Schmeing,T.M. and Ramakrishnan,V. (2009) What recent ribosome structures have revealed about the mechanism of translation. *Nature*, **461**, 1234–1242.
42. Bargis-Surgey,P., Lavergne,J.P., Gonzalo,P., Vard,C., Filhol-Cochet,O. and Reboud,J.P. (1999) Interaction of elongation factor eEF-2 with ribosomal P proteins. *Eur. J. Biochem.*, **262**, 606–611.
43. Vard,C., Guillot,D., Bargis,P., Lavergne,J.P. and Reboud,J.P. (1997) A specific role for the phosphorylation of mammalian acidic ribosomal protein P2. *J. Biol. Chem.*, **272**, 20259–20262.
44. Chan,S.H., Hung,F.S., Chan,D.S. and Shaw,P.C. (2001) Trichosanthin interacts with acidic ribosomal proteins P0 and P1 and mitotic checkpoint protein MAD2B. *Eur. J. Biochem.*, **268**, 2107–2112.
45. Too,P.H., Ma,M.K., Mak,A.N., Wong,Y.T., Tung,C.K., Zhu,G., Au,S.W., Wong,K.B. and Shaw,P.C. (2009) The C-terminal fragment of the ribosomal P protein complexed to trichosanthin reveals the interaction between the ribosome-inactivating protein and the ribosome. *Nucleic Acids Res.*, **37**, 602–610.
46. Chan,D.S., Chu,L.O., Lee,K.M., Too,P.H., Ma,K.W., Sze,K.H., Zhu,G., Shaw,P.C. and Wong,K.B. (2007) Interaction between trichosanthin, a ribosome-inactivating protein, and the ribosomal stalk protein P2 by chemical shift perturbation and mutagenesis analyses. *Nucleic Acids Res.*, **35**, 1660–1672.